ACS OMEGA

Article

Cite This: ACS Omega 2019, 4, 9361−9366

http://pubs.acs.org/journal/acsodf

Mitochondria-Targeted New Blue Light-Emitting Fluorescent Molecular Probe

Saswat Mohapatra,[†,‡,∥] Gaurav Das,[†,‡,∥] Chirantan Kar,[†,∥] Masashi Nitani,[§] Yutaka Ie,[§] Yoshio Aso,*[,§] and Surajit Ghosh*[,†,‡]

[†]Organic and Medicinal Chemistry Division, Structural Biology and Bioinformatics Division, CSIR-Indian Institute of Chemical Biology, 4 Raja S. C. Mullick Road, Jadavpur, Kolkata 700032, West Bengal, India

[‡]Academy of Scientific and Innovative Research (AcSIR), Chennai 201002, India

[§]The Institute of Scientific and Industrial Research Osaka University, 8-1, Mihogaoka, Osaka 567-0047, Ibaraki, Japan

Supporting Information

ABSTRACT: Discovery of a nontoxic fluorescent molecular probe to "light up" specific cellular organelles is extremely essential to understand dynamics of intracellular components. Here, we report a new nontoxic mitochondria-targeted linear bithiazole compound, containing trifluoroacetyl terminal groups, which emits intense blue fluorescence and stained mitochondria of various cells. Interestingly, the power of fluorescence is completely off when the bithiazole unit is stapled by a carbonyl bridge.

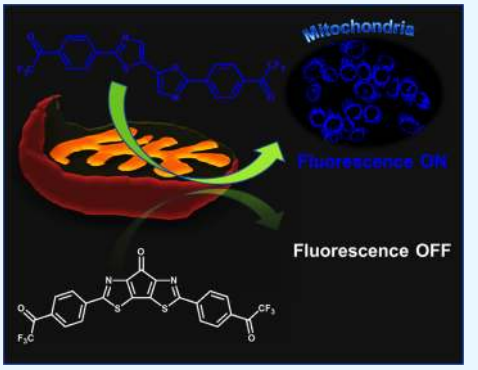

INTRODUCTION

Mitochondria are the highly populated organelles in all eukaryotic cells and have various cellular functions.[1,2] They act as the powerhouse of all the eukaryotic cells, as these essential organelles produce adenosine triphosphate (ATP), which is the key molecule for maintaining various cell functions.[3−5] Mitochondria's unique structural property containing a series of respiratory protein complexes, which maintain the electron flow and the redox balance through the respiratory chain, ultimately producing ATP.[6−8] Moreover, they also play a crucial role in the regulation of ion homeostasis and biogenesis of large intracellular molecules such as lipid and various free radicals.[3,6] Generally, the structure of healthy mitochondria is observed to have an oval shaped morphology and they are dynamic.[2] Slight perturbation in this crucial organelle causes various diseases such as cancer, neurodegenerative diseases, and metabolic disorders.[9] Therefore, visualization of mitochondria using a suitable probe can be considered as an easy strategy for monitoring the mitochondria and cellular health. There are few reports, which showed that a benzothiazolium-based NIR probe[10] and a benzothiadiazole-based fluorescence probe[11−13] target mitochondria. In addition, there are molecular probes which target mitochondrial H_2O_2[14−16] as well as act like fluorescence thermometers and molecular probes.[17−24] However, to the best of our knowledge, a mitochondria-targeted nontoxic blue light-emitting fluorescent probe is rare. Toward this venture, in this manuscript, we revealed a new mitochondria-targeted organic molecular probe (named as linear bithiazole: LBT), which can specifically illuminate the mitochondria of live cells with blue fluorescence. Interestingly, we also found that fluorescence of this molecule was completely off when the flexibility of this molecule was restricted by a carbonyl bridge [named as bridged bithiazole (BBT)].

RESULTS AND DISCUSSION

Here, we have used compounds containing a bithiazole unit and trifluoroacetyl terminal groups (LBT) and another carbonyl-bridged bithiazole unit and trifluoroacetyl terminal groups containing molecule (BBT) (Figure 1). Initially, we synthesized the molecule and characterized according to a previously described method.[25] Both the molecules exhibited absorbance maxima at 360 nm when dissolved in phosphate

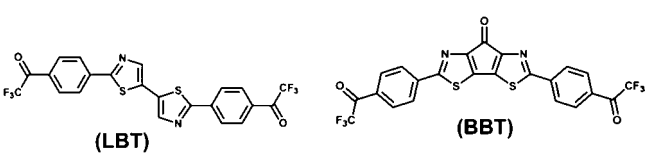

Figure 1. Chemical structure of LBT and BBT.

Received: November 29, 2018
Accepted: April 15, 2019
Published: May 29, 2019

DOI: 10.1021/acsomega.8b03331
ACS Omega 2019, 4, 9361−9366

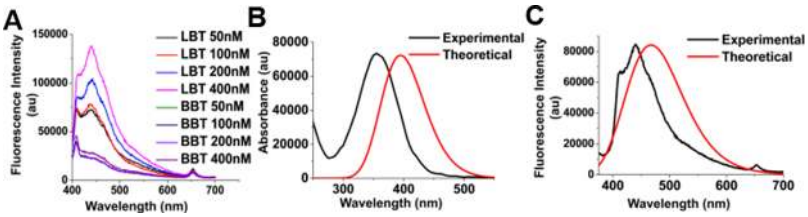

Figure 2. Fluorescence emission plot of LBT and BBT at various concentrations (A). Comparison of experimental and theoretical absorption (B)w and fluorescence emission (C) spectra of LBT. The Stokes shifts for experimental and theoretical spectra are 85 and 73, respectively.

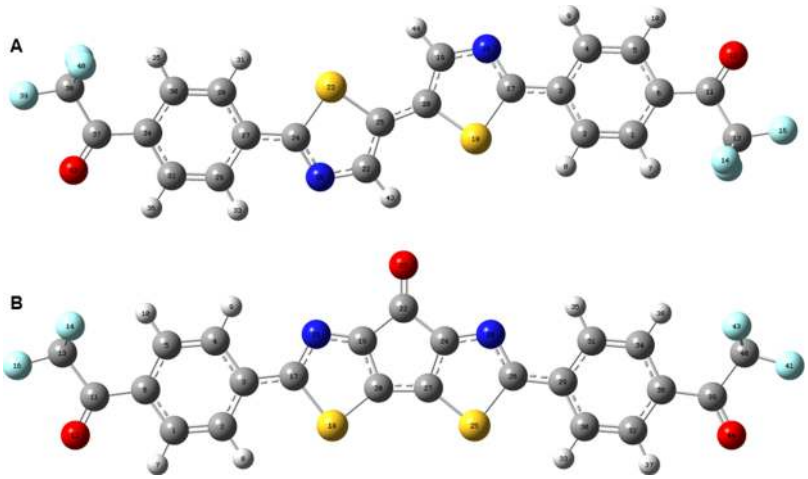

Figure 3. Geometry-optimized excited state of LBT (A) and BBT (B).

buffer saline; phosphate-buffered saline (PBS) (1×, pH = 7.4) (Figure S1).

Next, we have examined the emission fluorescence from both LBT and BBT. We have excited both BBT and LBT at 360 nm. Here, both the molecules are diluted with PBS (1×, pH = 7.4) of various concentrations like 50, 100, 200, and 400 nM. From the fluorescence intensity plot, we observed gradual concentration-dependent increase in fluorescence of LBT. Interestingly, BBT shows insignificant fluorescence in all the concentrations. The quantitative estimations reveal that LBT exhibits fivefold higher intensity as compared to BBT (Figure 2A).

We have also studied the photophysical properties of LBT. We found that it is soluble in water and dimethyl sulfoxide (DMSO). LBT exhibited a good quantum yield of 0.1211 and 46.5% photostability up to 24 h (Figure S2). We have also performed theoretical calculations to understand the absorbance and emission properties of both compounds LBT and BBT (Figure 2B,C). According to our experimental findings, we have assumed that the intense blue fluorescence of LBT at 440 nm is due to the probable delocalization of charge in the excited state between the five-membered rings and the terminal carbonyl groups. After comparing the geometries (Figures 3A and S3A) obtained from density functional theory (DFT) and calculation of both the ground state and the excited state of LBT, we can say that there is a significant change in the bond length of C5−C6, C4−C5, C3−C4, C3−C2, C2−C1, C1−C6, and C6−C11. This change in bond lengths indicates a probable charge transfer between the five-membered rings and the terminal carbonyl groups of LBT in the excited state. As expected, the theoretical and experimental UV/vis and emission spectra shown in Figure 2B,C are also in good agreement with each other.

In the case of BBT, the probability of similar charge delocalization between the five-membered rings and the terminal carbonyl groups is less because of the presence of the bridging carbonyl group near to the five-membered rings. Thus, the emission intensity of BBT is less compared to that of LBT. As evidenced from the DFT calculations, the change in bond lengths in the case of BBT (Figures 3B and S3B) is less when compared to that of LBT. All the important changes in the bond lengths of both the molecules LBT and BBT are shown in Table S1.

Furthermore, we have also shown the electrostatic potential distribution of the molecules (Figures S4 and 5) both in ground and excited states. Areas of high electron abundance and low potential are marked red, whereas areas of high potential and low electron abundance are marked as blue. As observed from Figure S4, the yellow to red color density around the terminal carbonyl group of BBT is less dark (both in excited and ground state) compared to that of the same in LBT. Thus, it is not surprising that the emission of LBT is much more intense than that of BBT in the same region (440 nm).

As we have observed, LBT is having characteristic fluorescence property; hence, we next evaluated whether LBT can be used as cellular dye or not. In the beginning, we have analyzed cellular uptake of the LBT using a flow cytometer (Figures 4A and S6). Here, HeLa cells were incubated with increasing concentration of LBT (10 nM, 100 nM, 1, 2, 4 and 10 μM) at 37 °C for 1 h. Then, the cells were evaluated with a flow cytometer instrument. The result is represented as fluorescence histogram overlay, which depicts increase in blue fluorescence in a concentration-dependent manner with respect to control or untreated cells. This increase

DOI: 10.1021/acsomega.8b03331
ACS Omega 2019, 4, 9361−9366

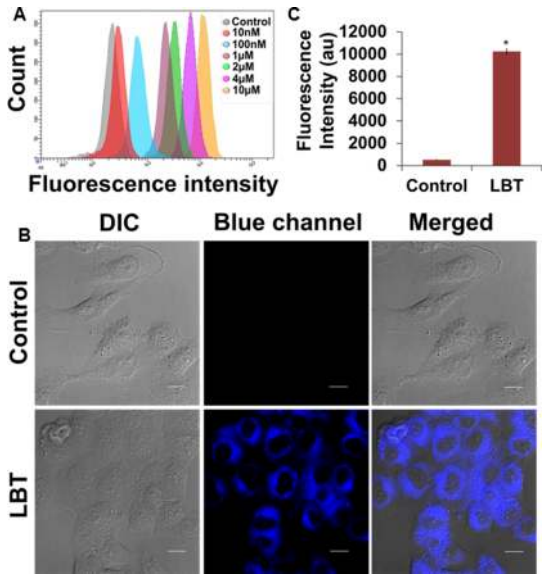

Figure 4. Flowcytometric uptake of LBT in HeLa cells at various concentrations (A). Microscopic analysis of LBT fluorescence in HeLa cells before (control) and after treatment of 1 μM of LBT (B). Scale bars correspond to 20 μm. Bar diagram-based representation of fluorescence emission intensity of microscopic data of HeLa cells before (control) and after (LBT; 1 μM) treatment (n = 10) (C). Data are shown as means ± standard deviation, *p < 0.001.

in blue fluorescence from cells indicate cellular localization of LBT.

The result also shows quite efficient uptake and fluorescence intensity at nanomolar concentration of LBT. Fluorescence property and cellular localization of LBT has made the molecule suitable for cellular dye. Hence, the next goal is to understand its cellular organelle or site specificity. Before this, toxicity of LBT has been analyzed using 3-(4,5-dimethylthiazol-2-yl)-2,5-diphenyltetrazolium bromide (MTT) assay (Figure S7A). Here, HeLa cells were harvested in 96 wells overnight followed by treating with LBT at various concentrations (0.5, 1, 2, and 4 μM) for 12 h. From the bar diagram, it can be confirmed that LBT has insignificant toxicity to cells. Further, toxicity against the cell has been analyzed by verifying the effect of LBT on the morphology of HeLa cells (Figure S7B). Here, cells were treated with 1 μM of LBT for 12 h. Then, cellular morphology has been analyzed under a microscope at the DIC mode. In comparison to untreated HeLa cells, LBT shows no characteristic changes of cellular morphology. Thus, LBT shows no change to cellular viability and cellular structure or morphology. Because of its nontoxic property, LBT could be used as a cell-staining agent in combination with other molecules, inhibitors, or cytotoxic molecules as well.

To understand specificity, we first checked cellular localization of LBT using a confocal microscope. Here, HeLa cells were cultured and harvested on bottom glass cover dish followed by incubation with LBT up to 1 h. Next, cells were washed with PBS (1×, pH = 7.4) and fresh medium was added. Then, cells were evaluated under a microscope in live conditions. Microscopy was carried out in DIC and blue channel mode. Here, untreated cells were considered as control. Microscopic images represent intense blue fluorescence staining of HeLa cells in comparison to control where no such fluorescence has been seen. Also, imaging in HeLa cells were performed along with BBT at 1 μM for 1 h, but again no fluorescence was observed (Figure S8). Intriguingly, this blue fluorescence is found to be localized at the cytoplasm near the nucleus and seems to be like a mitochondrial body (Figure 4A). Next, we have measured intensity of blue fluorescence from microscopic data. Here, we have observed significant increase in fluorescence in LBT-treated cells than control (Figure 4B). Because photo-damage and photo-bleaching are such evident problems in fluorescence microscopy, we have performed these experiments by irradiating HeLa cells with our dye for three and half hours and observed that till 24 h, no significant quenching or damage occurred, proving both the stability and the noncytotoxic nature of the dye (Figures S9 and S10).

Next, we tried to understand whether LBT is residing in mitochondria or not. For that, we have first stained the HeLa cell with 1 μM of LBT for 1 h, and then, cells were stained with mitotracker red (MTRC). Here, in comparison to LBT-untreated control cell, LBT-treated cells show higher blue fluorescence (Figures 5A,B and S11). Again, this blue

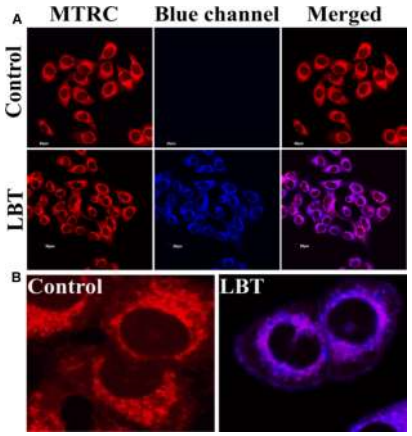

Figure 5. Confocal microscopic images showing colocalization of LBT with MTRC both at lower (A) and higher (B) magnification. Pearson's correlation coefficient $R(n)$ is 0.875. Scale bars correspond to 20 μm.

fluorescence is found to be colocalized with red fluorescence. This shows that LBT is also found to be accumulated in mitochondria as like MTRC. We have observed this phenomenon also through a real-time imaging as has been illustrated through a video that shows the colocalization of the mito-tracker with LBT over a course of 3 h and 40 min imaged at every 5 min interval (Supporting Information Video S1). We also observed that the mitochondrial localization of LBT slightly increases upon treatment of the cells with stimulants like carbonyl cyanide 4-(trifluoromethoxy)phenylhydrazone (FCCP), probably because of the depolarization of mitochondrial membrane potential (Figure S12). This has been studied through detailed analysis of their co-localization potential represented through the intensity correlation plot along with other important parameters (Figure S13, Table S2). Similar results also have been observed in the case of lung adenocarcinoma cancer (A549), glioblastoma (U-87MG), and mice melanoma (B16F10) cell lines where LBT colocalizes with mitochondria (Figure S14). From these confocal microscopic studies, it is confirmed that LBT is a blue fluorescence-emitting mitochondria staining agent. We have also checked the localization of BBT in lysosomes, but

DOI: 10.1021/acsomega.8b03331
ACS Omega 2019, 4, 9361−9366

unlike mitochondria, it does not show good co-localization with a lower Pearson coefficient (0.559). This proves the specificity of LBT for mitochondria as compared to other organelles (Figure S15).

Further, it is interesting to note that mitochondria are dynamic organelles and they undergo multiple cycles of fusion and fission, which offers mixing of key components and maintaining the number of mitochondria.[26] Mitochondria dynamicity also represents different conditions of the cells. Thus, a mitochondria-specific fluorescent probe could be an excellent tool for monitoring the dynamic states of mitochondria. Hence, we have used LBT with MTRC to monitor the different states of the mitochondrial structure such as filamentous, bead-like or longer filamentous structure. Here, in each of the case, we found mitochondrial localization of LBT (Figure 6A–C). Therefore, LBT can be used as a mitochondria-specific fluorescent probe.

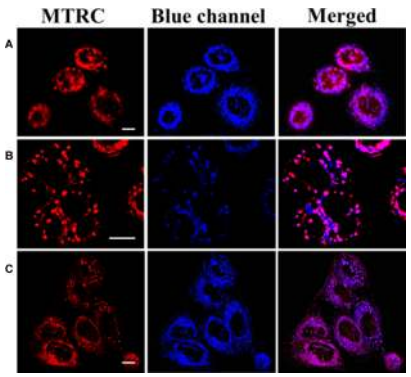

Figure 6. Confocal images of filamentous(A), bead-like (B), or both (C) structures of mitochondria. Pearson's correlation co-efficient $R(n)$ of the following structures are 0.908 (A), 0.829 (B), and 0.878 (C). Scale bars correspond to 20 μm.

CONCLUSIONS

In summary, we have discovered new nontoxic bithiazole containing a blue fluorescent mitochondrial probe (LBT), which shows photophysical property with 360 nm/440 nm (Ex/Em) in the blue fluorescence range. As very few blue fluorescence-emitting mitochondrial probes are available, LBT should be a suitable option for various cell-based fluorescence microscopy or flow cytometric analyses. Conversely, because of characteristic fluorescence features, LBT can be used for various Förster resonance energy transfer experiments with various fluorophores, such as cyan fluorescent protein, FITC, and GFP. Further, microscopic images reveal that this probe can monitor the different states of the mitochondrial structure. Therefore, this probe can be used as a new blue fluorescent mitotracker and has very high potential for cell biology and biochemistry research.

EXPERIMENTAL SECTION

Materials. DMSO and methanol (MeOH) were purchased from spectrochem. Triton X-100 was purchased from SRL. 2-[4-(2-Hydroxyethyl)piperazin-1-yl]ethanesulfonic acid was purchased from HiMedia. 5(6)-Carboxy fluorescence, MTT, Dulbecco's modified Eagle's medium (DMEM), MES, 4′,6-diamidino-2-phenylindole dihydrochloride, trypsin–ethylenediaminetetraacetic acid (EDTA) solution, DMSO for cell culture, and formaldehyde solution for molecular biology were purchased from Sigma-Aldrich. Anthracene was obtained from Spectrochem. MTRC (MitoTracker Red CMXRos)and LysoTracker Deep Red was procured from Thermo Fisher Scientific. FCCP was purchased from Abcam.

Methods. *Computational Analyses.* Full-geometry optimizations of the ground states were carried out using the density functional theory (DFT) method with the Becke-3-Lee-Yang-Parr (B3LYP) exchange functional and assigning the 6-31G** basis set. The absorbance spectra of the ground state of the molecules are calculated by time-dependent DFT (TDDFT) with the CAM-B3LYP exchange functional using the 6-31G** basis set. The emissive property of the excited states is calculated by complete geometry optimization by TDDFT with the CAM-B3LYP exchange functional using the 6-31G** basis set. For all the calculations, the solvent (water) was treated implicitly using the solvent model density model. All calculations were performed with the Gaussian '09 program with the help of the GaussView visualization program.[27] A preliminary conformation search using Spartan '18 has also been performed for both the molecules to choose the correct conformer.[28]

Fluorometric Analysis of LBT and BBT. Fluorescence emission of LBT and BBT were analyzed using a fluorometer at excitation 360 nm and the emission range of 400–700 nm at various concentrations.

Cells and Cell Culture. The human cervical cancer cell line (HeLa), lung adenocarcinoma cancer (A549), glioblastoma (U-87MG), and mice melanoma (B16F10) cell lines were collected from National Centre for Cell Science (NCCS) Pune, India. Then, cells were cultured and maintained under 5% CO_2 humidified incubator atmosphere at 37 °C using DMEM containing 10% fetal bovine serum, penicillin (50 units/mL), streptomycin (50 μg/mL), and kanamycin sulfate (110 mg/L). Trypsin–EDTA solution was used to digest the monolayer cell culture.

Cell Viability Analysis. Cell viability was performed by MTT assay using the standardized protocol.[29]

Cellular Uptake and Localization of LBT. Cells (1×10^6 cells/mL) were seeded in 6-well plates overnight. Then, cells were detached and taken in suspension. Next, cells were incubated with various concentrations of LBT (10 nM, 100 nM, 1, 2, 4, and 10 μM) for 1 h. Then, cells were given a PBS wash, and to it, pre-warmed media was added and analyzed using FACS.

For microscopic analysis of cellular uptake of LBT, HeLa cells were seeded on a glass bottom cover dish. Then, cells were incubated with 1 μM of LBT for 1 h. The cells were given a PBS wash and was analyzed under a microscope.

For mitochondria co-localization analysis, cells were seeded on a glass bottom cover dish overnight followed by treatment of 1 μM of LBT for 1 h. Then, cells were given a wash and incubated with 100 nM of MTRC (MitoTracker Red CMXRos) for 45 min followed by washes and fixation with 4% formaldehyde solution. Co-localization analysis was conducted under a confocal microscope. In the case of stimulation with FCCP, a mitochondrial oxidative phosphorylation uncoupler, before adding LBT, the cells were incubated with 20 nM FCCP for 1 h.

For lysosome localization analysis, cells were similarly seeded on a glass bottom cover dish overnight, followed by treatment of 1 μM of LBT for 1 h. Then, the cells were washed and incubated with 50 nM LysoTracker Deep Red for 30 min

DOI: 10.1021/acsomega.8b03331
ACS Omega 2019, 4, 9361–9366

followed by washing and fixation in 4% formaldehyde solution. Co-localization analysis as usual was conducted under a confocal microscope.

Real-Time Microscopic Live Cell Imaging. For live cell imaging, the HeLa cells grown overnight on confocal dishes were incubated with 100 nM of MTRC (MitoTracker Red CMXRos) for 45 min followed by washing and treatment with 1 μM of LBT which was then monitored for 3 h and 40 min and imaged at every 5 min in three channels (blue, TRITC and DIC) in a 5% CO_2 chamber of Tokai hit in an Olympus IX83 microscope equipped with an Andor (iXon3) EMCCD camera.

Photostability Experiment.[30] Photostability (dye photobleaching) of LBT was measured by exposing the dye to an incandescent light source for 24 h, and their fluorescence at 440 nm was measured at every 4 h interval up to 24 h.

Determination of Quantum Yield. The quantum yield was determined according to a previously described method.[31] Anthracene in ethanol (φ = 0.27) was used as the standard for the fluorescence quantum yield calculation as the emission of LBT is at 440 nm. In 1 cm quartz cuvettes, the fluorescence spectra and absorbance of both LBT and anthracene were measured.

Quantum yield was determined using the following equation

$$\varphi_{TC} = \varphi_{stand}(F_{TC}/F_{stand}) \times (A_{stand}/A_{TC}) \times ({n_{TC}}^2/{n_{stand}}^2)$$

φ = quantum yield, F = area under fluorescence spectra, A = absorption maxima, and n = refractive index.

Determination of Photo-Damage and Photo-Bleaching. This study has been performed following a previously described method.[32] Briefly, the HeLa cells treated with 1 μM LBT were irradiated under the blue channel of a fluorescence microscope for 3 h and 30 min. Thereafter, the cells were monitored and imaged at every 4 h interval in the DIC mode and blue channel for 24 h to observe any notable photo-damage caused to the cell photo-bleaching of the dye.

Microscope Parameter and Channel Information. All the images were taken under similar exposure time for control and LBT-treated cells (281.2 and 280.2 ms respectively). EM gain and gain were maintained as value 10.0 and 1.0, respectively. Lamp intensity was 5.40. For LBT and BBT, the excitation/emission filters are 360/440 nm; for the MTRC channel, it is 579/599 nm, and for LysoTracker Deep Red, it is 647/668 nm (excitation and emission class both near IR).

■ ASSOCIATED CONTENT

Supporting Information

The Supporting Information is available free of charge on the ACS Publications website at DOI: 10.1021/acsomega.8b03331.

Experimental details and additional data (PDF)

Real-time imaging showing co-localization of mitochondria with LBT (MPG)

■ AUTHOR INFORMATION

Corresponding Authors

*E-mail: aso@sanken.osaka-u.ac.jp (Y.A.).

*E-mail: sghosh@iicb.res.in (S.G.).

ORCID

Gaurav Das: 0000-0002-8432-5384

Yutaka Ie: 0000-0003-0208-4298

Surajit Ghosh: 0000-0002-8203-8613

Author Contributions

‖S.M., G.D., and C.K. contributed equally.

Notes

The authors declare no competing financial interest.

■ ACKNOWLEDGMENTS

S.M. thanks UGC fellowship. G.D. thanks ICMR fellowship. C.K. acknowledges SERB for the post-doctoral fellowship and Dr. Saumik Sen for his unconditional support. A special thanks to Krishnangsu Pradhan for his help in the photophysical studies of LBT. S.G. kindly acknowledges DBT, India (BT/PR19159/NNT/1043/2016), for providing full financial support and CSIR-IICB for infrastructure. S.G. and Y.A. thank DST, India, and JSPS, Japan, for initiating this project under the Indo-Japan Science Cooperative Program.

■ REFERENCES

(1) Alberts, B.; Bray, D.; Hopkin, K.; Johnson, D. A.; Lewis, J.; Raff, M.; Roberts, K.; Walter, P. *Essential Cell Biology*, 4th ed.; Garland Science, 2013.

(2) Cottet-Rousselle, C.; Ronot, X.; Leverve, X.; Mayol, J.-F. Cytometric Assessment of Mitochondria Using Fluorescent Probes. *Cytometry, Part A* **2011**, *79*, 405−425.

(3) Johnson, L. V.; Walsh, M. L.; Chen, L. B. Localization of mitochondria in living cells with rhodamine 123. *Proc. Natl. Acad. Sci. U.S.A.* **1980**, *77*, 990−994.

(4) Pagliarini, D. J.; Calvo, S. E.; Chang, B.; Sheth, S. A.; Vafai, S. B.; Ong, S.-E.; Walford, G. A.; Sugiana, C.; Boneh, A.; Chen, W. K.; Hill, D. E.; Vidal, M.; Evans, J. G.; Thorburn, D. R.; Carr, S. A.; Mootha, V. K. A mitochondrial protein compendium elucidates complex I disease biology. *Cell* **2008**, *134*, 112−123.

(5) Sickmann, A.; Reinders, J.; Wagner, Y.; Joppich, C.; Zahedi, R.; Meyer, H. E.; Schonfisch, B.; Perschil, I.; Chacinska, A.; Guiard, B.; Rehling, P.; Pfanner, N.; Meisinger, C. The proteome of Saccharomyces cerevisiae mitochondria. *Proc. Natl. Acad. Sci. U.S.A.* **2003**, *100*, 13207−13212.

(6) Masanta, G.; Lim, C. S.; Kim, H. J.; Han, J. H.; Kim, H. M.; Cho, B. R. A Mitochondrial-Targeted Two-Photon Probe for Zinc Ion. *J. Am. Chem. Soc.* **2011**, *133*, 5698−5700.

(7) Friedman, J. R.; Nunnari, J. Mitochondrial form and function. *Nature* **2014**, *505*, 335−343.

(8) Perry, S. W.; Norman, J. P.; Barbieri, J.; Brown, E. B.; Gelbard, H. A. Mitochondrial membrane potential probes and the proton gradient: a practical usage guide. *BioTechniques* **2011**, *50*, 98−115.

(9) Nunnari, J.; Suomalainen, A. Mitochondria: In Sickness and in Health. *Cell* **2012**, *148*, 1145−1159.

(10) Abeywickrama, C. S.; Baumann, H. J.; Alexander, N.; Shriver, L. P.; Konopka, M.; Pang, Y. NIR-emitting benzothiazolium cyanines with an enhanced stokes shift for mitochondria imaging in live cells. *Org. Biomol. Chem.* **2018**, *16*, 3382−3388.

(11) Neto, B. A. D.; Carvalho, P. H. P. R.; Santos, D. C. B. D.; Gatto, C. C.; Ramos, L. M.; Vasconcelos, N. M. d.; Corrêa, J. R.; de Oliveira, H. C. B.; Silva, R. G.; Silva, R. G. Synthesis, properties and highly selective mitochondria staining with novel, stable and superior benzothiadiazole fluorescent probes. *RSC Adv.* **2012**, *2*, 1524−1532.

(12) Zou, Q.; Tian, H. Chemodosimeters for mercury(II) and methylmercury(I) based on 2,1,3-benzothiadiazole. *Sens. Actuators, B* **2010**, *149*, 20−27.

(13) Carvalho, P. H. P. R.; Correa, J. R.; Guido, B. C.; Gatto, C. C.; De Oliveira, H. C. B.; Soares, T. A.; Neto, B. A. D. Designed Benzothiadiazole Fluorophores for Selective Mitochondrial Imaging and Dynamics. *Chem.—Eur. J.* **2014**, *20*, 15360−15374.

(14) Dai, F.; Jin, F.; Long, Y.; Jin, X. L.; Zhou, B. A 1,8-naphthalimide-based turn-on fluorescent probe for imaging mitochon-

DOI: 10.1021/acsomega.8b03331
ACS Omega 2019, 4, 9361−9366

drial hydrogen peroxide in living cells. *Free Radic. Res.* **2018**, *52*, 1288−1295.
(15) Xu, J.; Zhang, Y.; Yu, H.; Gao, X.; Shao, S. Mitochondria-Targeted Fluorescent Probe for Imaging Hydrogen Peroxide in Living Cells. *Anal. Chem.* **2016**, *88*, 1455−1461.
(16) Yang, L.; Li, N.; Pan, W.; Yu, Z.; Tang, B. Real-Time Imaging of Mitochondrial Hydrogen Peroxide and pH Fluctuations in Living Cells Using a Fluorescent Nanosensor. *Anal. Chem.* **2015**, *87*, 3678−3684.
(17) Arai, S.; Suzuki, M.; Park, S.-J.; Yoo, J. S.; Wang, L.; Kang, N.-Y.; Ha, H.-H.; Chang, Y.-T. Mitochondria-targeted fluorescent thermometer monitors intracellular temperature gradient. *Chem. Commun.* **2015**, *51*, 8044−8047.
(18) Yang, X.; Liu, W.; Tang, J.; Li, P.; Weng, H.; Ye, Y.; Xian, M.; Tang, B.; Zhao, Y. A multi-signal mitochondria-targeted fluorescent probe for real-time visualization of cysteine metabolism in living cells and animals. *Chem. Commun.* **2018**, *54*, 11387−11390.
(19) Shchepinova, M. M.; Cairns, A. G.; Prime, T. A.; Logan, A.; James, A. M.; Hall, A. R.; Vidoni, S.; Arndt, S.; Caldwell, S. T.; Prag, H. A.; Pell, V. R.; Krieg, T.; Mulvey, J. F.; Yadav, P.; Cobley, J. N.; Bright, T. P.; Senn, H. M.; Anderson, R. F.; Murphy, M. P.; Hartley, R. C. MitoNeoD: A Mitochondria-Targeted Superoxide Probe. *Cell Chem. Biol.* **2017**, *24*, 1285−1298.
(20) Li, K.; Hou, J.-T.; Yang, J.; Yu, X.-Q. A tumor-specific and mitochondria-targeted fluorescent probe for real-time sensing of hypochlorite in living cells. *Chem. Commun.* **2017**, *53*, 5539−5541.
(21) He, L.; Yang, X.; Xu, K.; Lin, W. A mitochondria-targeted fluorescent probe for imaging endogenous malondialdehyde in HeLa cells and onion tissues. *Chem. Commun.* **2017**, *53*, 4080−4083.
(22) Huang, H.; Dong, F.; Tian, Y. Mitochondria-Targeted Ratiometric Fluorescent Nanosensor for Simultaneous Biosensing and Imaging of O2- and pH in Live Cells. *Anal. Chem.* **2016**, *88*, 12294−12302.
(23) Zhang, J.; Bao, X.; Zhou, J.; Peng, F.; Ren, H.; Dong, X.; Zhao, W. A mitochondria-targeted turn-on fluorescent probe for the detection of glutathione in living cells. *Biosens. Bioelectron.* **2016**, *85*, 164−170.
(24) Liu, Y.; Li, K.; Wu, M.-Y.; Liu, Y.-H.; Xie, Y.-M.; Yu, X.-Q. A mitochondria-targeted colorimetric and ratiometric fluorescent probe for biological SO2 derivatives in living cells. *Chem. Commun.* **2015**, *51*, 10236−10239.
(25) Ie, Y.; Nitani, M.; Karakawa, M.; Tada, H.; Aso, Y. Air-Stable n-Type Organic Field-Effect Transistors Based on Carbonyl-Bridged Bithiazole Derivatives. *Adv. Funct. Mater.* **2010**, *20*, 907−913.
(26) Chen, H.; Chan, D. C. Mitochondrial dynamics-fusion, fission, movement, and mitophagy-in neurodegenerative diseases. *Hum. Mol. Genet.* **2009**, *18*, R169−R176.
(27) Frisch, J. M.; et al. *Gaussian 09*, Revision D.01; Gaussian Inc.: Wallingford CT, 2013.
(28) Kong, J.; White, C. A.; Krylov, A. I.; Sherrill, D.; Adamson, R. D.; Furlani, T. R.; Lee, M. S.; Lee, A. M.; Gwaltney, S. R.; Adams, T. R.; Ochsenfeld, C.; Gilbert, A. T. B.; Kedziora, G. S.; Rassolov, V. A.; Maurice, D. R.; Nair, N.; Shao, Y.; Besley, N. A.; Maslen, P. E.; Dombroski, J. P.; Daschel, H.; Zhang, W.; Korambath, P. P.; Baker, J.; Byrd, E. F. C.; Van Voorhis, T.; Oumi, M.; Hirata, S.; Hsu, C.-P.; Ishikawa, N.; Florian, J.; Warshel, A.; Johnson, B. G.; Gill, P. M. W.; Head-Gordon, M.; Pople, J. A. Q-Chem 2.0: a high-performanceab initio electronic structure program package. *J. Comput. Chem.* **2000**, *21*, 1532−1548.
(29) Mohapatra, S.; Saha, A.; Mondal, P.; Jana, B.; Ghosh, S.; Biswas, A.; Ghosh, S. Synergistic Anticancer Effect of Peptide-Docetaxel Nanoassembly Targeted to Tubulin: Toward Development of Dual Warhead Containing Nanomedicine. *Adv. Healthc. Mater.* **2017**, *6*, 1600718.
(30) Dar, M.; Giesler, T.; Richardson, R.; Cai, C.; Cooper, M.; Lavasani, S.; Kille, P.; Voet, T.; Vermeesch, J. Development of a novel ozone- and photo-stable HyPer5 red fluorescent dye for array CGH and microarray gene expression analysis with consistent performance irrespective of environmental conditions. *BMC Biotechnol.* **2008**, *8*, 86.
(31) Lakowicz, J. R. *Principles of Fluorescence Spectroscopy*, 3rd ed.; Springer, 2010.
(32) Wäldchen, S.; Lehmann, J.; Klein, T.; van de, L. S.; Sauer, M. Light-induced cell damage in live-cell super-resolution microscopy. *Sci. Rep.* **2015**, *5*, 15348.

DOI: 10.1021/acsomega.8b03331
ACS Omega 2019, 4, 9361−9366